IEEE Access
Multidisciplinary | Rapid Review | Open Access Journal

Received December 10, 2018, accepted January 8, 2019, date of publication January 21, 2019, date of current version March 4, 2019.

Digital Object Identifier 10.1109/ACCESS.2019.2894011

Analysis and Suppression for Frequency Oscillation in a Wind-Diesel System

HAIXIN WANG[1], JUNYOU YANG[1], ZHE CHEN[2], (Senior Member, IEEE), WEICHUN GE[3], YUNLU LI[1], YIMING MA[1], JIAN DONG[1], MARTIN ONYEKA OKOYE[1], AND LIJIAN YANG[4]

[1]School of Electrical Engineering, Shenyang University of Technology, Shenyang 110870, China
[2]Department of Energy Technology, Aalborg University, 9220 Aalborg, Denmark
[3]Liaoning Province Electric Power Company, Shenyang 110006, China
[4]School of Information Science and Engineering, Shenyang University of Technology, Shenyang 110870, China

Corresponding author: Junyou Yang (junyouyang@sut.edu.cn)

ABSTRACT In a wind-diesel system with weak network architecture, many techniques are utilized to enhance its stability. However, the frequency oscillation between the grid-side converter and the diesel generator may be caused by their interactions, and there are only a few studies considering this issue, which is a major challenge for the stability. To tackle this challenge, the cause of frequency oscillation is studied, and an adaptive fuzzy PI controller based on the variable universe is proposed to suppress oscillation in this paper. The control parameter of the wind turbine generator (WTG) converter's dc-link voltage loop and wind speed has an important influence on the oscillation. Our main idea is to suppress frequency oscillation by the optimizing control parameter. In order to analyze the interaction between WTG and diesel generator, we develop the small-signal models of the wind-diesel generator. Subsequently, the adaptive fuzzy PI controller based on the variable universe is proposed in the dc-link voltage loop to optimize control parameter instead of gain-scheduled PI controller, and its key feature is the innovative use of an extension factor with d-axis current in the output universe. The function of the extension factor is to adapt WTG to different wind speeds. The experimental results demonstrate that the proposed controller can significantly suppress frequency oscillation. The oscillation amplitude of isolated grid frequency is also significantly reduced by up to 0.175 Hz.

INDEX TERMS Frequency oscillation, fuzzy PI controller, wind turbine generator (WTG), variable universe, wind-diesel system.

I. INTRODUCTION

With the rapid development of renewable energy, a large number of power electronic devices are connected to the power system. The increasing of installed capacity of wind power brings power system new challenges of operation and control. Especially in a wind-diesel system, the capacity of power electronic devices accounts for a large proportion. Due to poor adaptability of the device controllers and the interactions between the devices and the wind-diesel system, frequency oscillations are easily caused, which need to be improved [1]–[3].

At present, some studies on wind turbine generator (WTG) oscillation can be broadly categorized into various classes. **a)** Oscillations caused by self-characteristic of WTG. Reference [4] considered wind shear and tower shadow effects in WTGs. Such oscillation is called a 3p oscillation, which can cause shaft torsion load aggravation and shaft torque oscillation, and inevitably leads to electromagnetic torque and power fluctuations in the generator [5]. **b)** Sub-synchronous resonance (SSR) oscillations. SSR oscillations in nearby wind turbine-generators connected to series capacitive compensated transmission systems were studied [6]–[8]. Furthermore, references [9], [10] pointed out some rules of SSR problems in wind farm. **c)** Inter-area oscillations. Inter-area oscillations of WTGs and interconnected system were researched [11], [12]. The level of oscillation was related to the output power of WTGs [13]. In this paper, a new oscillation problem caused by the interactions between WTGs and the weak grid is one of the major challenges for system stability, which is less studied.

Currently, there are many analysis methods for frequency oscillation. **a)** Modal identification method was applied to discriminate and analyze the real-time monitoring waveform

The associate editor coordinating the review of this manuscript and approving it for publication was Ton Do.

of oscillation. Frequency and damping information of the oscillation mode were obtained, but the mode shape information was inaccessible [14]. **b)** Impedance analysis method considered the converter and grid as two independent subsystems, and the system stability was quantitatively analyzed by using port external characteristics [15]. **c)** Bifurcation theory was mainly used to analyze the nonlinear singularity of power system near the critical point. From the mathematical spatial structure, bifurcation theory combines eigenvalues with high order polynomials to analyze the system stability, but the calculation is complex [16]. **d)** Eigenvalue analysis based on the principle of small perturbation judged the original system whether stable or not, which has become one of the most effective low-frequency oscillation analysis methods in a multi-machine system [17].

Power system stabilizer (PSS) and power oscillation damper (POD) are generally used in the suppression of power system oscillation [14], [18]–[21]. However, these methods are mainly designed to suppress inter-area oscillations, which belong to upper-level dispatching strategies. This paper tackles the oscillations between DC-link capacitor of the grid-side converter (GSC) of permanent magnet synchronous generator (PMSG)-based wind turbine and the diesel generator in an isolated grid, as the above strategies are inappropriate. Generally, gain scheduled PI (GSPI) controller is one of the most popular methods in the DC-link voltage control loop of GSC [22]–[24]. In this paper, the frequency oscillation is caused by the interaction between WTG and the diesel generator. DC-link voltage and wind speed are two factors that influence the oscillation. DC-link voltage is applied in the GSPI controller. However, wind speed is not considered. Moreover, the fuzzy control theory has the advantage of optimizing PI control parameter [25], [26]. Therefore, this paper optimizes control parameter based on fuzzy control theory to mitigate the oscillation in a wind-diesel system. The contributions with respect to the proposed control algorithms are as follows.

- To suppress frequency oscillation, this paper develops an adaptive fuzzy PI controller based on the variable universe, which proposes an extension factor with d-axis current in the output universe. The function of the extension factor is to add wind speed to the optimization of the control parameter.
- Based on oscillation phenomena and eigenvalue analysis of a small-signal model of the wind-diesel system, it is found that the control parameter has an influence on the oscillation. With the increasing of wind speed, the amplitude of oscillation decreases.
- Comparing with the state-of-the-art GSPI control, the oscillation amplitude of isolated grid frequency and DC-link voltage with the proposed method are significantly reduced by up to 0.175 Hz and nearly 10 V respectively.

This paper is organized as follows. Section II describes the oscillation phenomena in an isolated wind-diesel grid. Section III uses the small-signal model to analyze the wind-diesel system. The proposed fuzzy PI controller is designed in section IV. The experiment results are shown in Section V. Finally, the conclusion is drawn in Section VI.

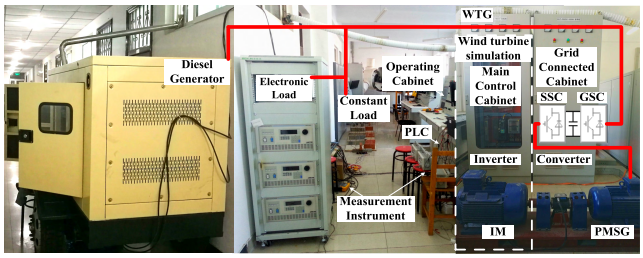

FIGURE 1. The isolated grid framework.

II. MOTIVATION

A. ISOLATED WIND-DIESEL GRID FRAMEWORK

The isolated grid includes a diesel generator, a PMSG-based wind turbine, and load. The isolated grid framework is shown in Fig. 1. The role of a diesel generator is to support isolated grid voltage and frequency. The PMSG-based wind turbine is simulated by an indoor WTG. The indoor WTG consists of operating cabinet, grid-connected cabinet, main control cabinet, induction motor (IM) and PMSG. The driving system of wind turbine simulation is composed of inverter and IM. The output of IM is adjusted by the inverter. IM drags PMSG running. The output power of PMSG is fed to the isolated grid through the converter. The maximum power point tracking (MPPT) is achieved by stator-side converter (SSC). DC-link voltage is stabilized by GSC. The wind turbine simulation algorithm is applied to PLC. According to wind speed, pitch angle and generator speed, wind turbine mechanical power are calculated by (1).

$$\begin{cases} P_m = 0.5\rho C_p(\lambda, \beta) A_r V_w^3, \\ C_p(\lambda, \beta) = c_1(c_2/\lambda_i - c_3\beta - c_4)e^{-c_5/\lambda_i} + c_6\lambda, \\ \dfrac{1}{\lambda_i} = \dfrac{1}{\lambda + 0.08\beta} - \dfrac{0.035}{\beta^3 + 1}, \\ \lambda = \dfrac{\omega_r}{V_w}, \end{cases} \tag{1}$$

where P_m is mechanical power, ρ is air density, C_p is the power coefficient, λ is the tip speed ratio, β is the pitch angle, A_r is the effective area covered by turbine blades, V_w is wind speed, c_1, c_2, c_3, c_4, c_5 and c_6 are coefficients. ω_r is the generator-angular speed. Wind speed is obtained by a look-up table or I external input. The pitch angle control system is also simulated in PLC.

The overall control block diagrams of the isolated wind-diesel grid are shown in Fig. 2. P_e is output power of PMSG-based wind turbine, P_d is output power of diesel generator and P_l is load power. Power deviation P_{dev} is the sum of P_e, P_d, and P_l. Then frequency deviation f_{dev} is obtained by frequency dynamic model $H_g(s)$, while M is inertia coefficient and D is damping coefficient. The diesel generator is controlled to balance grid power flow. The governor and engine

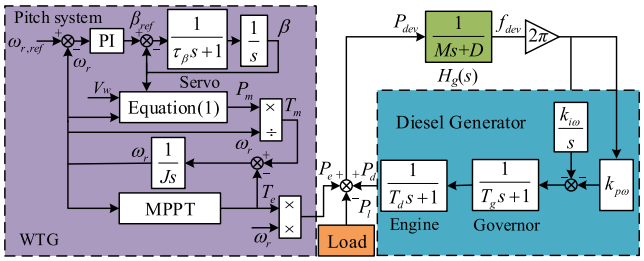

FIGURE 2. The isolated grid control block diagram.

TABLE 1. Parameters of isolated grid.

Systems	Parameters	Values
Diesel engine	Rated power	13.5 kW
Diesel generator	Rated power	10 kW
	Rated frequency	50 Hz
	T_d	0.005 s
	T_g	0.1 s
Constant load	Rated power	4.5 kW
Electronic load	Rated power	10 kW
Wind turbine	Rated wind speed	12 m/s
	Blade radius	2.53 m
PMSG	Rated power	9 kW
	Rated angular speed	38.4 rad/s
	L_f	5 mH
	C_f	31.4 μF
	J	0.0375 kg·m^2
Wind-diesel system	M	0.5
	D	0.01

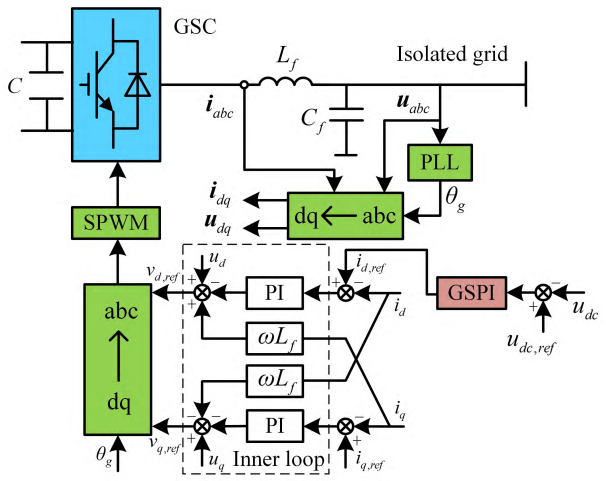

FIGURE 3. Control block diagram of GSC.

dynamics of diesel generator are modeled as in [27]. T_d and T_g are time constants of engine and governor respectively. $k_{p\omega}$ and $k_{i\omega}$ are controller parameters of diesel generator. In the pitch system of WTG, β_{ref} is a reference value of pitch angle, τ_β is the mechanical time constant of pitch servo, and the classical PI controller is to stabilize the WTG speed at the reference $\omega_{r,ref}$. ω_r is obtained by rotor motion equation. T_m is mechanical torque, and J is a moment of inertia. Isolated grid parameters are shown in Table 1.

The control strategy of GSC is shown in Fig. 3. C is the DC-link capacitance, L_f and C_f are inductance and capacitance of filter respectively, $\boldsymbol{i}_{abc}$ is the output current, $\boldsymbol{u}_{abc}$ is the grid voltage, $\boldsymbol{i}_{dq}$ and $\boldsymbol{u}_{dq}$ are the current and voltage in dq coordinate system respectively, θ_g is the phase angle obtained by phase-locked loop (PLL), ω is the grid angle frequency. In the inner loop, $i_{d,ref}$ and $i_{q,ref}$ are the d-axis and q-axis current references respectively. In the outer loop, $u_{dc,ref}$ and u_{dc} are the reference value and actual value of DC-link voltage respectively. $v_{d,ref}$ and $v_{q,ref}$ are output voltage references of GSC, and can be calculated by (2).

$$\begin{cases} v_{d,ref} = H_i(s)(i_{d,ref} - i_d) + u_d - \omega L_f i_q \\ v_{q,ref} = H_i(s)(i_{q,ref} - i_q) + u_q + \omega L_f i_{gd} \end{cases} \tag{2}$$

where $H_i(s)$ is the transfer function of current loop. When reactive power is not required, $i_{q,ref}$ is set to zero. Then $i_{d,ref}$ is obtained by the state-of-the-art GSPI control. The GSPI controller can be expressed by (3).

$$i_{d,ref} = G_k(u_{dc,ref} - u_{dc})(k_{pdc} + \frac{k_{idc}}{s}), \tag{3}$$

where G_k is the gain based on DC-link voltage deviation.

B. MOTIVATIONAL EXPERIMENTS

In experiments, when V_w is 0 m/s, 8 m/s and 12 m/s, WTG is connected to the large power grid and isolated wind-diesel grid respectively. Experimental results under each case are shown in Fig. 4 and Fig. 5. When V_w is 0 m/s, there is no output power from SSC, and GSC control signals are enabled to stabilize the DC-link voltage at its reference value. When V_w is 8 m/s and 12m/s, the output power of WTG is fed to the large power grid or isolated grid. When WTG is connected to the large power grid, experimental results are shown in Fig. 4. When WTG is connected to the isolated wind-diesel grid, the experimental results are shown in Fig. 5.

When wind speed is 0 m/s in Fig. 4, it can be seen that the relevant variables of WTG are stable when WTG is connected to the large power grid. Comparing i_q and $i_{q,ref}$ in Fig. 4(a) with those in Fig. 5(a), there is no significant difference. However, oscillation amplitudes of the other variables increase gradually in Fig. 5(d)(g)(j). The fluctuation of $i_{d,ref}$ and i_d in Fig. 5(d) is more obvious than those in Fig. 4(d). Compared with u_{dc} in Fig. 4(g), u_{dc} in Fig. 5(g) fluctuates severely. Meanwhile, compared with Fig. 4(j), u_q in Fig. 4(j) fluctuates violently. When wind speed is 8 m/s, the reference of d-axis current $i_{d,ref}$ is increased to regulate output power. In Fig. 4(e)(h)(k), the relevant variables of WTG are stable when WTG is connected to the large power grid. However, when WTG is connected to the isolated wind-diesel grid, oscillation phenomena of i_d, $i_{d,ref}$, u_{dc} and $u_{dc,ref}$ are also generated as shown in Fig. 5(e)(h)(k).

At the wind speeds of 0 and 8 m/s, when WTG is connected to the isolated grid, it causes the severe oscillation phenomena. In the inner loop, due to the PI controller as shown in Fig. 3, current responses are rapid. It can be seen that $i_q$is stable at $i_{q,ref}$ which is zero. i_d is changed with its reference $i_{d,ref}$. The fluctuation of $i_{d,ref}$ is caused by the deviation between $u_{dc,ref}$ and u_{dc}, which leads to the variation

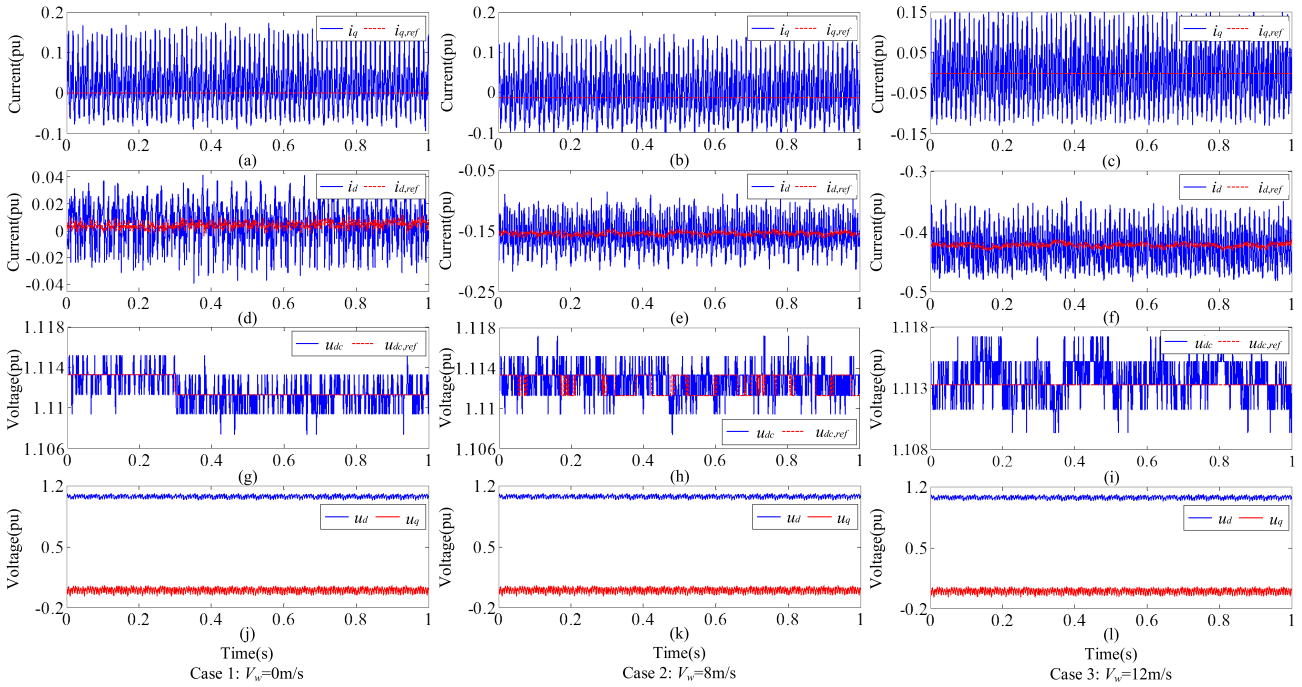

FIGURE 4. Experimental results in the large power grid with the GSPI controller. (a)-(c) q-axis current and its reference of GSC in three cases. (d)-(f) d-axis current and its reference of GSC in three cases. (g)-(i) DC-link voltage of GSC in three cases. (j)-(l) d-q axis voltages of grid in three cases.

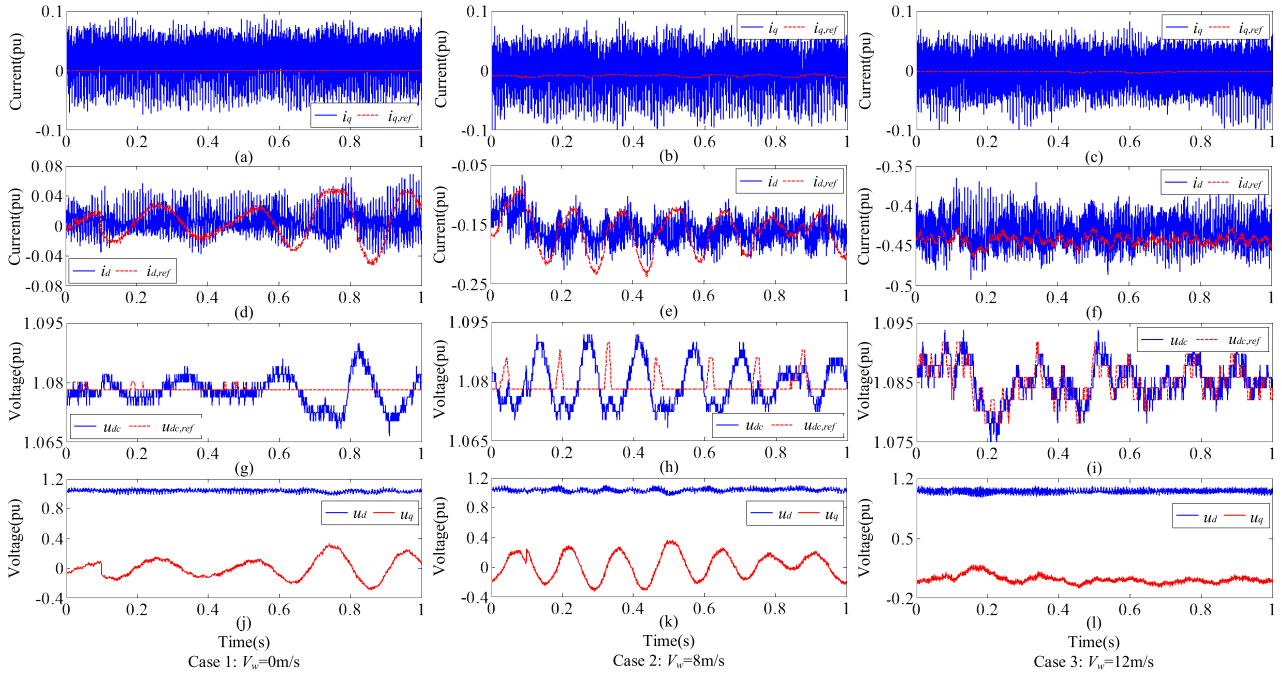

FIGURE 5. Experimental results in isolated grid with the GSPI controller. (a)-(c) q-axis current and its reference of GSC in three cases. (d)-(f) d-axis current and its reference of GSC in three cases. (g)-(i) DC-link voltage of GSC in three cases. (j)-(l) d-q axis voltages of grid in three cases.

of output power. Furthermore, the rapid change of output power of WTG has an important influence on the voltage and frequency of the isolated grid. Thus, the fluctuation of u_q is caused which is obtained by PLL. As we know, u_q is normally zero. According to the control algorithm shown in Fig. 3, the variation of u_q affects the output voltage of GSC and aggravates the oscillation.

When V_w is 12 m/s, WTG runs at the rated power, and the experimental results are shown in Fig. 4(c)(f)(i)(l) and Fig. 5(c)(f)(i)(l). In Fig. 4(c)(f)(i)(l), WTG is connected to the

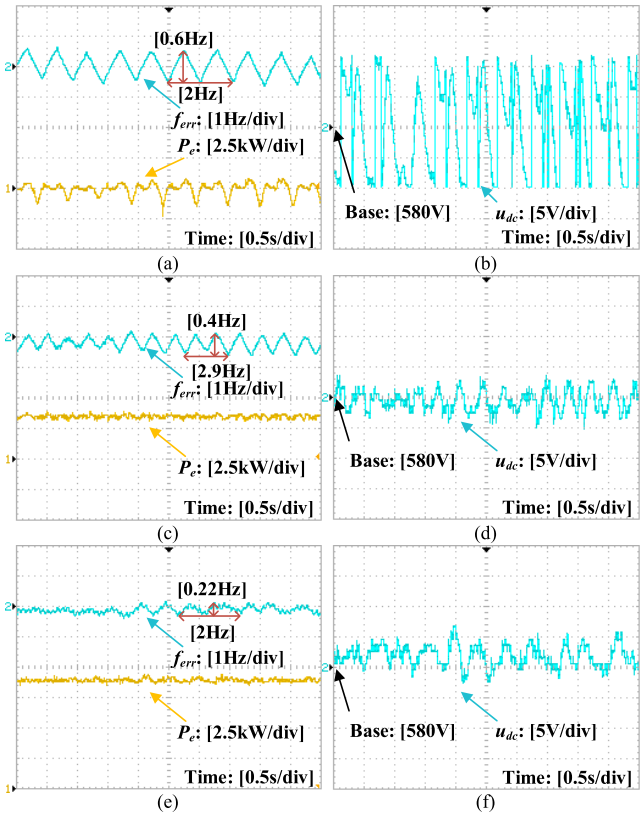

FIGURE 6. f_{err}, P_e and u_{dc} curves in isolated grid with the GSPI controller. (a)-(b) When $V_w = 0$m/s. (c)-(d) When $V_w = 8$m/s. (e)-(f) When $V_w = 12$m/s.

large power grid, and the operation of WTG is also stable. Compared with case 1 and case 2 in Fig. 5, the oscillation amplitudes of relevant variables of case 3 in Fig. 5 are reduced. Though u_{dc} has a certain fluctuation, u_{dc} is very close to $u_{dc,ref}$. As a result, $i_{d,ref}$, i_d, u_d and u_q have little variations. In case 3, WTG operation remains relatively stable. u_d and u_q are calculated by the Clark and Park transforms based on the measured grid three-phase voltage. In large power grid, the grid voltage and frequency are generally constant regardless of wind speed changes. Thus, u_d and u_q are also constant. However, in isolated grid, when wind power changes, the voltage and frequency of the wind-diesel system are influenced, then u_d and u_q are changed. At the rated wind speed, wind power is almost constant, then u_d and u_q are essentially unchanged.

In Fig. 6, frequency deviation f_{dev}, output power P_e and DC-link voltage u_{dc} are compared at different cases. Fig. 6(a) and (b) show the experimental results when wind speed V_w is 0 m/s. The variation of f_{dev} is severe. Oscillation frequency and amplitude of f_{dev} are 2 Hz and 0.3 Hz respectively. u_{dc} fluctuation amplitude is up to 10 V, and P_e fluctuates severely around zero. The DC-link capacitances are rapidly charging or discharging. When V_w is 8 m/s, the experimental results are shown in Fig. 6(c) and (d). Oscillation frequency and amplitude of f_{dev} are 2.9 Hz and 0.2 Hz respectively. P_e is

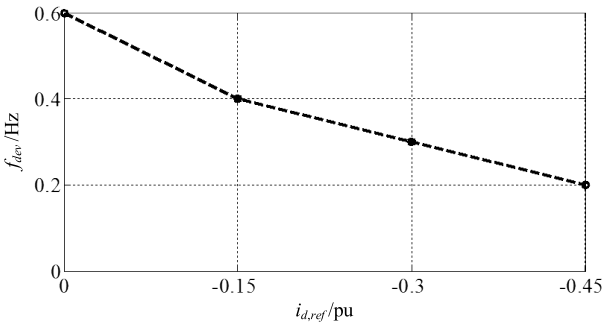

FIGURE 7. The relationship of $i_{d,ref}$ and f_{dev} in the isolated wind-diesel grid.

about 3 kW, and fluctuation amplitude of u_{dc} is less than that when V_w is 0 m/s. The oscillation amplitude of f_{dev} in Fig. 6(c) is smaller than that in Fig. 6 (a). When V_w is 12 m/s, the results are shown in Fig. 6(e) and (f). Oscillation frequency and amplitude of f_{dev} are 2 Hz and 0.11 Hz respectively, f_{dev} is significantly better than Fig. 6 (a) and (c). P_e is about 9 kW, and u_{dc} in Fig. 6(f) is of small fluctuation. The relationship between oscillation amplitude of f_{dev} and $i_{d,ref}$ is obtained as shown in Fig. 7. It can be seen that the oscillation amplitude of $f_{dev}$is decreased with increasing absolute value of $i_{d,ref}$, which keeps a linear relationship.

C. ANALYSIS OF THE OSCILLATION

It can be seen that when WTG is connected to the large power grid, there has no oscillation under the three cases. When WTG is connected to the isolated grid, oscillation phenomenon is caused. Due to constant wind speed, the output power of SSC is constant. Thus, the causation of oscillation in the wind-diesel isolated grid is not the power fluctuation of the wind turbine. It can be seen from Fig. 4, and 5, i_q is relatively stable, not the major influencing factor of oscillation. i_d also responds rapidly. The deviation of u_{dc} and $u_{dc,ref}$ is large. Thus, in the wind-diesel isolated grid, the immediate cause of oscillation is the variation of u_{dc}. GSPI parameter of the DC-link voltage control loop is inadequate at different wind speeds. At low wind speed, GSPI controller leads to $i_{d,ref}$ fluctuation, and P_e is influenced. The change of isolated grid frequency makes a contribution to variations of u_d and u_q in PLL. At the same time, frequency fluctuation also has a corresponding impact in the inner loop, further exacerbates the oscillation. In the vicinity of rated power, the GSPI controller is in a saturated state, and the output power of WTG is relatively stable.

The impedance of the large power grid is very small and can be ignored, but the impedance of the diesel generator is relatively large. Thus, the impedance characteristic of the wind-diesel system is analyzed. We represent the WTG by a Norton equivalent circuit, in the form of a current source (i_s) in parallel with an impedance (Z_{gsc}). The load is represented by its impedance (Z_{load}). Z_{par} is the parallel impedance of Z_{gsc} and Z_{load}. The diesel generator is represented by

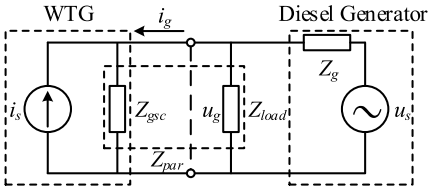

FIGURE 8. Representation of the wind-diesel system.

a Thevenin equivalent circuit, in the form of a voltage source (u_s) in series with an impedance (Z_g) [28], [29]. The representation of the wind-diesel system is shown in Fig. 8.

In Fig. 8, i_g is output current of WTG, u_g is grid output voltage. According to the equivalent circuit, equation (4) is derived.

$$i_g(s) = \frac{1}{Z_{par}(s) + Z_g(s)} u_s(s) - \frac{Z_{par}(s)}{Z_{par}(s) + Z_g(s)} i_s(s). \quad (4)$$

In order to suppress the influence of grid voltage on the grid-connected current, it is necessary to increase the modulus of $Z_{par}(s) + Z_g(s)$. Furthermore, when$Z_g(s)$ and $Z_{load}(s)$ are constant, improving $Z_{gsc}(s)$ has an important effect on enhancing the anti-disturbance performance of GSC. Generally, under the unity power factor operation assumption, the impedance matrix $Z_{gsc}(s)$ can be diagonalized. The gain variations of GSPI and PLL would result in a variation of impedance matrix $Z_{gsc}(s)$. In this paper, the synchronous reference frame PLL (SRF-PLL) is adopted, which is one of the most basic and popular PLLs for grid synchronization. Thus, the key point is to change control parameters of GSPI to optimize the impedance characteristics of GSC.

Further physical analysis of the oscillation is made. The major energy storage elements of GSC and diesel generator are capacitors and inductors respectively. WTG is equivalent to capacitor C and negative resistor ($R < 0$) at the oscillation frequency. The diesel generator is equivalent to inductor L. Therefore, the wind-diesel isolated grid could be regarded as an L-C-R second-order negative damping oscillation circuit. Due to the negative resistance effect, power is generated by the negative resistor, and power oscillation begins to diverge. When it diffuses to the limit, equal amplitude oscillation is generated. If the capacitor voltage exceeds its reference value, the capacitor releases energy, the inductor absorbs energy, and the rotor speed of diesel generator increases. If the capacitor voltage goes below its reference value, the capacitor absorbs energy, the inductor releases energy, and the rotor speed of diesel generator speed decreases.

III. ANALYSIS OF SMALL-SIGNAL STABILITY

Small-signal stability of wind-diesel isolated grid is analyzed. The output power of WTG is the main cause of the oscillation. Since GSC of WTG is often operated with unity power factor, the output power of WTG is reflected in the d-axis current. Within a certain range of the stable operating point, G_k is almost constant, and (4) can be written as (5).

$$i_{d,ref} = (u_{dc,ref} - u_{dc})(k_{pdc} + \frac{k_{idc}}{s}), \quad (5)$$

where k_{pdc} and k_{idc} are proportional and integral coefficients of GSPI controller respectively. The DC-link power is expressed by (6).

$$u_{dc} C \frac{du_{dc}}{dt} = P_s + 1.5(u_d i_d + u_q i_q), \quad (6)$$

where P_s is the PMSG output power. In order to simplify the analysis, some realistic assumptions and approximations are made in the models. Due to the rapid response of internal loop of GSC, assuming that $i_d = i_{d,ref}$, $i_q = i_{q,ref} = 0$, and u_d is constant within the small-signal fluctuation, equations (5) and (6) are linearized, and the small-signal dynamic models of WTG is obtained by (7) when P_s is constant.

$$\begin{cases} \Delta\dot{i}_{dI} = k_{idc}(\Delta u_{dc,ref} - \Delta u_{dc}), \\ \Delta i_d = k_{pdc}(\Delta u_{dc,ref} - \Delta u_{dc}) + \Delta i_{dI}, \\ \Delta\dot{u}_{dc} \\ = \dfrac{\Delta P_s + 1.5(u_{d0}\Delta i_d + i_{d0}\Delta u_d + u_{q0}\Delta i_q + i_{q0}\Delta u_q)}{C u_{dc0}}, \end{cases} \quad (7)$$

where 'Δ' indicates a small-signal value around the operating point, subscript '0' indicates steady-state value around the operating point. The role of diesel generator in the isolated grid is to regulate frequency by its output power. Diesel generator's mechanical power reference $P_{dm,ref}$ is obtained by (8).

$$P_{dm,ref} = (\omega_{ref} - \omega)(k_{p\omega} + \frac{k_{i\omega}}{s}), \quad (8)$$

where H is inertia coefficient of diesel generator, and P_{dm} is mechanical power. To simplify the analysis, assuming $P_{dm} = P_{dm,ref}$, the small-signal dynamic models of diesel generator are obtained by (9).

$$\begin{cases} \Delta\dot{P}_{dmI} = k_{p\omega}(\Delta\omega_{ref} - \Delta\omega), \\ \Delta P_{dm} = k_{idc}(\Delta\omega_{ref} - \Delta\omega) + \Delta P_{dmI}, \\ \Delta\dot{\omega} = \dfrac{\Delta P_{dm} - \Delta P_d}{H\omega_0}. \end{cases} \quad (9)$$

According to (7) and (9), the state equation of wind-diesel system is obtained by (10).

$$\begin{bmatrix} \Delta\dot{i}_{dI} \\ \Delta\dot{u}_{dc} \\ \Delta\dot{P}_{dmI} \\ \Delta\dot{\omega} \end{bmatrix} = \begin{bmatrix} 0 & -k_{idc} & 0 & 0 \\ \dfrac{1.5u_{d0}}{Cu_{dc0}} & \dfrac{-1.5u_{d0}k_{pdc}}{Cu_{dc0}} & 0 & 0 \\ 0 & 0 & 0 & -k_{i\omega} \\ \dfrac{-1.5u_{d0}}{H\omega_0} & \dfrac{1.5u_{d0}k_{pdc}}{H\omega_0} & \dfrac{1}{H\omega_0} & \dfrac{-k_{p\omega}}{H\omega_0} \end{bmatrix} \times \begin{bmatrix} \Delta i_{dI} \\ \Delta u_{dc} \\ \Delta P_{dmI} \\ \Delta\omega \end{bmatrix}. \quad (10)$$

In this model, different parameters of the DC-link voltage controller are selected, and the eigenvalues are calculated as shown in Table 2 and Table 3. DC-link voltage controller

TABLE 2. Wind diesel system eigenvalues when $k_{pdc} = 3.5$.

k_{idc}	λ_1	λ_2	λ_3	λ_4
20	-2.53+j6.569	-2.53-j6.569	-1.971+j0.920	-1.971-j0.920
50	-2.53+j10.841	-2.53-j10.841	-1.971+j0.920	-1.971-j0.920
100	-2.53+j15.54	-2.53-j15.54	-1.971+j0.920	-1.971-j0.920
150	-2.53+j19.115	-2.53-j19.115	-1.971+j0.920	-1.971-j0.920
180	-2.53+j20.971	-2.53-j20.971	-1.971+j0.920	-1.971-j0.920

TABLE 3. Wind diesel system eigenvalues when $k_{idc} = 100$.

k_{pdc}	λ_1	λ_2	λ_3	λ_4
2.5	-0.51+j15.736	-0.51-j15.736	-1.971+j0.920	-1.971-j0.920
3	-1.52+j15.671	-1.52-j15.671	-1.971+j0.920	-1.971-j0.920
3.5	-2.53+j15.54	-2.53-j15.54	-1.971+j0.920	-1.971-j0.920
4	-3.548+j15.34	-3.548+j15.34	-1.971+j0.920	-1.971-j0.920
4.5	-4.561+j15.07	-4.561+j15.07	-1.971+j0.920	-1.971-j0.920

parameters have influences on the eigenvalues λ_1 and λ_2. λ_3 and λ_4 are mainly affected by the parameters of diesel generator controller. Therefore, in order to analyze the influence of DC-link voltage controller parameters, λ_3 and λ_4 are ignored.

In Table 2, the control parameter k_{pdc} is set as a constant value. With the increasing k_{idc}, the imaginary parts of λ_1 and λ_2 are variable and their real parts are constant. In Table 3, the control parameter k_{idc} is set as a constant value. With the increasing k_{pdc}, the real parts of λ_1 and λ_2 are variable, and the imaginary parts are constant. The real parts of eigenvalues have a major effect on system stability. It can be seen that k_{pdc} has a great impact on system stability. If k_{pdc} is too large, i_d overshooting may be caused. If k_{pdc} is too small, the improper adjustment may lead to increasing oscillation. Therefore, the optimization of the control parameter k_{pdc} has a great influence on the system stability. k_{pdc} is related to the variation of DC-link voltage deviation based on (3). According to the experimental results in Fig. 5, the DC-link voltage deviation is severe at low wind speeds, k_{pdc} is changed frequently and inappropriately. At high wind speeds, the DC-link voltage deviation is slight. In the small-signal model, unsuitable selection of k_{pdc} will affect the system stability. Thus, besides DC-link voltage deviation, different wind speeds also need to be considered to adjust k_{pdc}.

IV. THE PROPOSED VARIABLE UNIVERSE FUZZY PI CONTROLLER

In order to improve the system stability, a variable universe fuzzy PI controller is presented to optimize k_{pdc} to suppress the oscillation of u_{dc}. The fuzzy PI control algorithm is shown in Fig. 9. $u_{dc,err}$ and $du_{dc,err}/dt$ are input variables of the fuzzy controller. α is a contraction-expansion factor, which is to adapt WTG to the conditions of different wind speeds. The adjustment of proportional coefficient Δk_{pdc} is calculated by the variable universe fuzzy PI controller, which includes fuzzifier, fuzzy inference machine and defuzzifier.

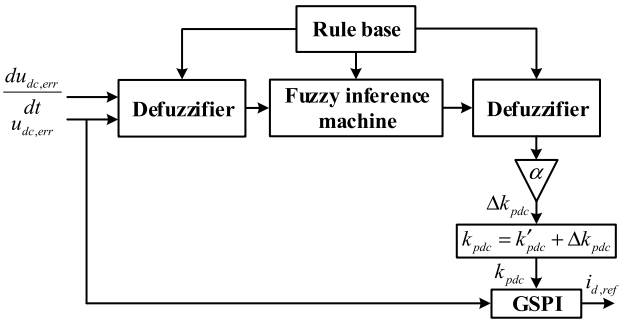

FIGURE 9. Block diagram of the variable universe fuzzy PI controller.

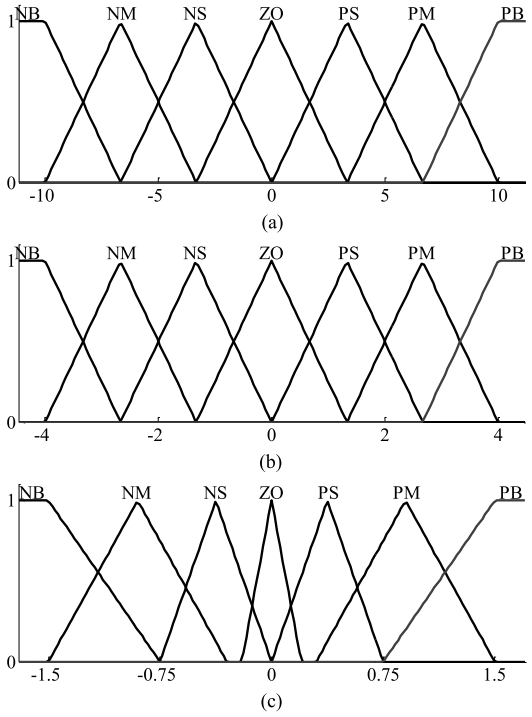

FIGURE 10. Membership functions. (a) Membership functions of $u_{dc,err}$. (b) Membership functions of $d_{udc,err/dt}$ (c) Membership functions of Δk_{pdc}.

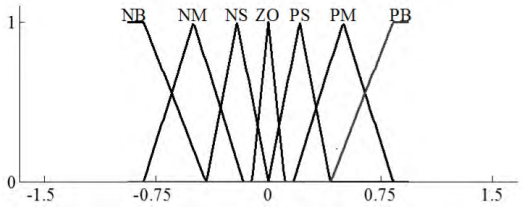

FIGURE 11. Membership functions of Δk_{pdc}.

k'_{pdc} is the initial parameter. Through the modification of k_{pdc}, when the grid frequency oscillates, the DC-link voltage of GSC can be more stable and robust.

For simplicity of application, the normal, consistent, and complete fuzzy sets with the triangular membership functions are often considered for input and output variables [30],

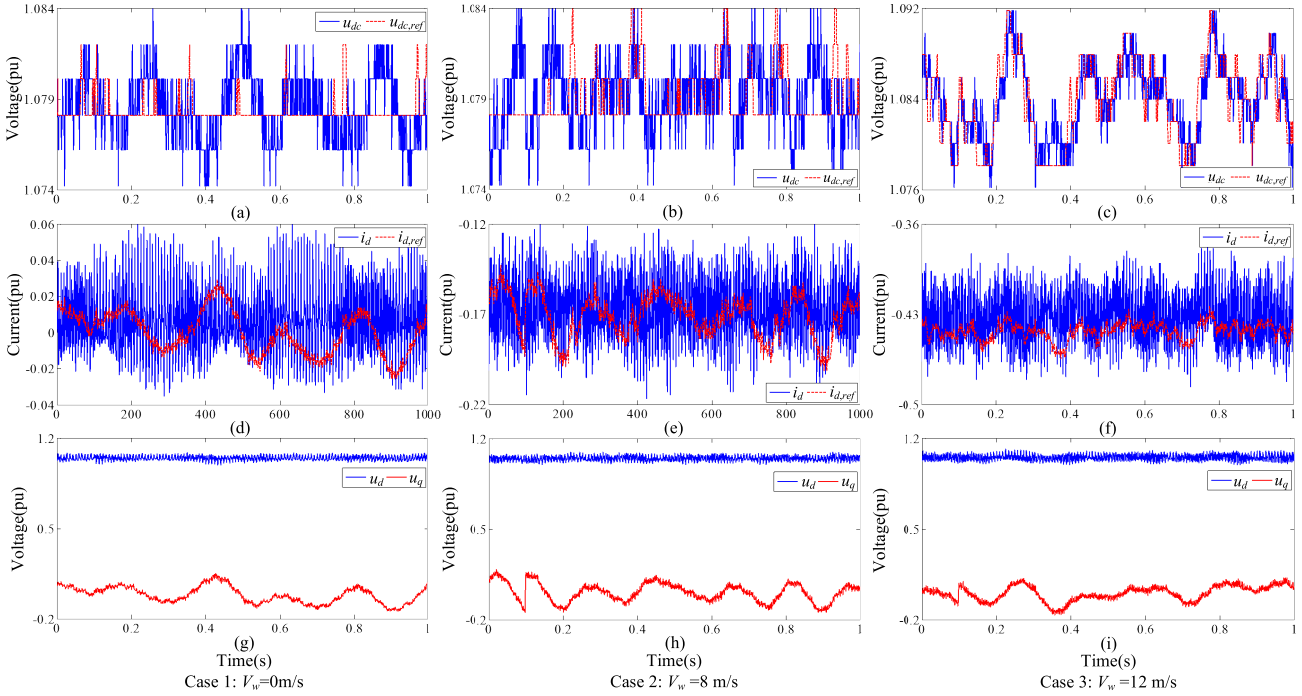

FIGURE 12. Experimental results in isolated grid with the variable universe fuzzy PI controller. (a)-(c) DC-link voltage of GSC in three cases. (d)-(f) d-axis current and its reference of GSC at three cases. (g)-(i) d-q axis voltages of isolate grid in three cases.

although other shapes such as the bell, Gaussian and trapezoid which are used to describe the membership functions, can also be selected. The universe of $u_{dc,err}$ is set as [−10V, 10V], the universe of $du_{dc,err}/dt$ is set as [−4, 4], and the universe of Δk_{pdc} is set as [−1.5, 1.5]. Furthermore, fuzzifier performs a mapping from crisp inputs and output to their fuzzy sets. The universes of $u_{dc,err}$ and$du_{dc,err}/dt$ on their fuzzy sets are defined as {−3, −2, −1, 0, 1, 2, 3}, and the universe of Δk_{pdc} on a fuzzy set is defined as {−3, −2, −1, 0, 1, 2, 3}. The corresponding fuzzy subsets are defined as {negative big (NB), negative median (NM), negative small (NS), zero (ZO), positive small (PS), positive median (PM), positive big (PB)}. The membership functions are shown in Fig. 10. In fuzzy set theory, the fuzzy sets are characterized by their triangular membership functions, which assign to each element a number in the interval 0 to 1. This represents the grade of membership. The steeper the shape of a triangle, the higher the control sensitivity in the corresponding universe. In the universe of flat shapes, the control system will be more robust. Thus, when we design the triangle shapes of output membership, the steeper triangle is adopted in the universe of smaller error, and the flatter triangle is used in the universe of larger error. Generally, the variable universe means that input or output universes can change according to the changing of their variables. However, based on the above motivational experiments and analysis, the output power of WTG is a major impact factor of the oscillation phenomena in this wind-diesel system. i_d can characterize the variation of output power. Furthermore, in order to obtain adequate control parameters for adapting the conditions of different

TABLE 4. Fuzzy control rules.

$du_{dc,err}/dt$ / $u_{dc,err}$	NB	NM	NS	ZO	PS	PM	PB
NB	PB	PB	PM	PM	PS	PS	ZO
NM	PB	PB	PM	PS	PS	ZO	NS
NS	PM	PM	PM	PS	ZO	NS	NS
ZO	PM	PM	PS	ZO	NS	NM	NM
PS	PS	PS	ZO	NS	NS	NM	NM
PM	PS	ZO	NS	NM	NM	NB	NB
PB	ZO	NS	NM	NM	NM	NB	NB

WTG output power, considering the characteristics of linear relationship of the wind-diesel system in Fig. 7, we propose a contraction-expansion factor α in output universe of the fuzzy PI controller as shown in (11).

$$\alpha = (1 - \frac{i_d}{i_{d,\max}}) + \varepsilon, \tag{11}$$

where ε is a sufficiently small positive number, $\varepsilon = 10^{-4}$. The design of αshould follow the principle of duality, monotonicity, coordination, normality and zero avoidance. The contraction-expansion factor can be defined as the adjustment of language control variable universe. Its output universe is transformed into $[-1.5\alpha, 1.5\alpha]$, and new membership function is shown in Fig. 11.

Rule base consists of a collection of fuzzy IF-THEN rules. According to engineering experience, the fuzzy rules formulated in this paper are shown in Table 4.

Based on the input variables and fuzzy control rules, fuzzy inference machine performs a mapping from fuzzy sets of input variables to fuzzy sets of the output variable. Mamdani method is used to reason the synthesis rules. Finally,

defuzzifier maps output fuzzy set to a crisp value. Here, we use the weighted average method to obtain Δk_{pdc} as shown in (12).

$$M_{avr} = \frac{\sum_{i=1}^{n} U(u_i)u_i}{\sum_{i=1}^{n} U(u_i)} \tag{12}$$

where M_{avr} is the crisp output of the fuzzy system, $u_i (i = 1, 2.....n)$ is an element of output fuzzy set, and $U(u_i)$ is the responding membership function value. When $u_{dc,err}$ changes, Δk_{pdc} is adjusted by the fuzzy PI controller, which ensures that u_{dc} tracks $u_{dc,ref}$ stably. Compared with the existing GSPI controller, the variable universe fuzzy PI controller adapts WTG to the conditions of different wind speeds, and exhibits better robustness in suppressing u_{dc} oscillation.

V. EXPERIMENT

Experimental platform and its specific control block diagram are shown in Fig. 1 and Fig. 2 respectively. The variable universe fuzzy PI controller is verified below in three cases. Different wind speeds are set, and the power of load and diesel generator are constant. The experimental results are shown in Fig. 12 and Fig. 13.

A. CASE 1: $V_W = 0$ m/s

In this case, PMSG does not generate power to SSC, and GSC utilizes isolated grid power to stabilize DC-link voltage. GSPI controller exhibits poor performances in Fig. 5. The experimental results adopted the variable universe fuzzy PI controller are shown in Fig. 12(a), (d) and (g). Due to the adjustment Δk_{pdc}, the deviation of u_{dc} and $u_{dc,ref}$ in Fig. 12(a) is less than that in Fig.5 (d), which shows that u_{dc} can stably track $u_{dc,ref}$ based on the fuzzy controller. The oscillations of i_d and $i_{d,ref}$ in Fig. 12(d) are also weakened, and i_d is around zero. u_d and u_q in Fig. 12(g) are more stable than those in Fig. 5(j). Fig. 13(a) and (b) show the curves of P_e, f_{err} and u_{dc}. It can be seen that the oscillations of f_{err} and u_{dc} are smaller than those in Fig. 6(a) and (b), and P_e is also around zero. Compared with the GSPI controller, the overall oscillation amplitude of u_{dc} is lowered by nearly 10 V. The oscillation amplitude of f_{err} is reduced by up to 0.175 Hz. The wind-diesel system is relatively more stable.

B. CASE 2: $V_W = 8$ m/s

In this case, the WTG operates in the MPPT mode. Fig. 12(b), (e), and (h) show the experimental results with the fuzzy PI controller. u_{dc} and $u_{dc,ref}$ in Fig. 12(b) are more stable than those in Fig. 5(h), and its oscillation amplitudes are similar to those in Fig. 12(a). i_d in Fig. 12(e) is close to -0.17 pu. The adjustable range of Δk_{pdc} has already been narrowed according to equation (11). Fig. 13(c) and (d) show the curves of P_e, f_{err}, u_{dc} when $V_w = 8$ m/s. Compared with Fig. 7(c) and (d), it can be seen that the power oscillation of GSC is reduced, the oscillation amplitudes of f_{err} and u_{dc} are also decreased, and the system stability is enhanced.

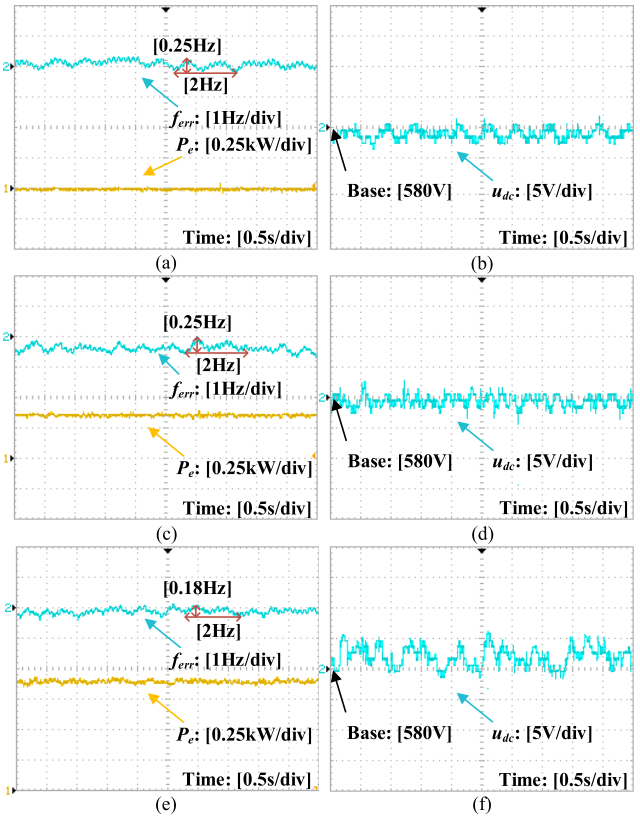

FIGURE 13. f_{err}, P_e and u_{dc} curves in isolated grid with the variable universe fuzzy PI controller. (a)-(b) When $V_W = 0$m/s. (c)-(d) When $V_W = 8$m/s. (e)-(f) When $V_W = 12$m/s.

C. CASE 3: $V_W = 12$ m/s

In this case, WTG is in the rated power operating condition. Fig. 12(c), (f) and (i) show the experimental results with the variable universe fuzzy PI controller. In Fig. 12(b), u_{dc} tracks $u_{dc,ref}$ tightly. According to equation (11), i_d is close to $i_{d,max}$, and α is small when $V_w = 12$ m/s. When u_{dc} changes, Δk_{pdc} has a small adjustment. The fuzzy PI controller plays a fine-tuning role, and the initial parameters play the main role. Our expected target is achieved. Fig. 13(e) and (f) show the curves of P_e, f_{err}, u_{dc} when $V_w = 12$ m/s. Compared with Fig. 7(e) and (f), it can be seen that P_e and are u_{dc} stable.

VI. CONCLUSIONS

Oscillation causes of the isolated grid are researched, and an adaptive fuzzy PI controller is proposed. The theoretical analysis and experimental results show that the control parameters of DC-link voltage controller and wind speed are related to the oscillations, and more especially k_{pdc} has large influences on the stability of frequency and WTG output power. Thus, only k_{pdc} is adjusted by the fuzzy PI controller. Besides, with decreasing wind speed, the oscillation is more severe. By building the extension factor of the output universe with i_d, the adjustment of k_{pdc} is increased at low wind speeds and decreased at high wind speeds. Compared with the state-of-the-art GSPI controller, the oscillation amplitude of isolated

grid frequency is significantly reduced by up to 0.175 Hz, and the oscillation amplitude of DC-link voltage is substantially reduced by nearly 10 V. The proposed fuzzy PI controller plays a certain inhibitory effect on system oscillation.

REFERENCES

[1] M. Mokhtari and F. Aminifar, "Toward wide-area oscillation control through doubly-fed induction generator wind farms," *IEEE Trans. Power Syst.*, vol. 29, no. 6, pp. 2985–2992, Nov. 2014.

[2] Y. Liu, J. R. Gracia, T. J. King, and Y. Liu, "Frequency regulation and oscillation damping contributions of variable-speed wind generators in the U.S. Eastern interconnection (EI)," *IEEE Trans. Sustain. Energy*, vol. 6, no. 3, pp. 951–958, Jul. 2015.

[3] A. E. Leon and J. A. Solsona, "Sub-synchronous interaction damping control for DFIG wind turbines," *IEEE Trans. Power Syst.*, vol. 30, no. 1, pp. 419–428, Jan. 2015.

[4] W. Hu, C. Su, and Z. Chen, "Impact of wind shear and tower shadow effects on power system with large scale wind power penetration," in *Proc. 37th Annu. Conf. IEEE Ind. Electron. Soc. (IECON)*, Melbourne, VIC, Australia, Nov. 2011, pp. 878–883.

[5] Z. Xie, Z. Xu, X. Zhang, S. Yang, and L. Wang, "Improved power pulsation suppression of DFIG for wind shear and tower shadow effects," *IEEE Trans. Ind. Electron.*, vol. 64, no. 5, pp. 3672–3683, May 2017.

[6] L. Fan, R. Kavasseri, Z. L. Miao, and C. Zhu, "Modeling of DFIG-based wind farms for SSR analysis," *IEEE Trans. Power Del.*, vol. 25, no. 4, pp. 2073–2082, Oct. 2010.

[7] L. Fan, C. Zhu, Z. Miao, and M. Hu, "Modal analysis of a DFIG-based wind farm interfaced with a series compensated network," *IEEE Trans. Energy Convers.*, vol. 26, no. 4, pp. 1010–1020, Dec. 2011.

[8] Z. Miao, "Impedance-model-based SSR analysis for type 3 wind generator and series-compensated network," *IEEE Trans. Energy Convers.*, vol. 27, no. 4, pp. 984–991, Dec. 2012.

[9] S. O. Faried, I. Unal, D. Rai, and J. Mahseredjian, "Utilizing DFIG-based wind farms for damping subsynchronous resonance in nearby turbine-generators," *IEEE Trans. Power Syst.*, vol. 28, no. 1, pp. 452–459, Feb. 2013.

[10] M. S. El-Moursi, B. Bak-Jensen, and M. H. Abdel-Rahman, "Novel STATCOM controller for mitigating SSR and damping power system oscillations in a series compensated wind park," *IEEE Trans. Power Electron.*, vol. 25, no. 2, pp. 429–441, Feb. 2010.

[11] A. Arvani and V. S. Rao, "Power oscillation damping controller for the power system with high wind power penetration level," in *Proc. North Amer. Power Symp. (NAPS)*, Pullman, WA, USA, 2014, pp. 1–6.

[12] H. H. Askari, S. Hashemi, R. Eriksson, and Q. Wu, "Effect of full converter wind turbines on inter-area oscillation of power systems," in *Proc. Int. Conf. Clean Elect. Power (ICCEP)*, Taormina, Italy, 2015, pp. 270–276.

[13] J. Morató, T. Knüppel, and J. Østergaard, "Residue-based evaluation of the use of wind power plants with full converter wind turbines for power oscillation damping control," *IEEE Trans. Sustain. Energy*, vol. 5, no. 1, pp. 82–89, Jan. 2014.

[14] T. Knüppel, J. N. Nielsen, K. H. Jensen, A. Dixon, and J. Østergaard, "Power oscillation damping capabilities of wind power plant with full converter wind turbines considering its distributed and modular characteristics," *IET Renew. Power Gener.*, vol. 7, no. 5, pp. 431–442, Sep. 2013.

[15] K. M. Alawasa, Y. A.-R. I. Mohamed, and W. Xu, "Modeling, analysis, and suppression of the impact of full-scale wind-power converters on subsynchronous damping," *IEEE Syst. J.*, vol. 7, no. 4, pp. 700–712, Dec. 2013.

[16] W. Zhu, R. R. Mohler, R. Spee, W. A. Mittelstadt, and D. Maratukulam, "Hopf bifurcations in a SMIB power system with SSR," *IEEE Trans. Power Syst.*, vol. 11, no. 3, pp. 1579–1584, Aug. 1996.

[17] L. Wang, X. Xie, Q. Jiang, and H. R. Pota, "Mitigation of multimodal subsynchronous resonance via controlled injection of supersynchronous and subsynchronous currents," *IEEE Trans. Power Syst.*, vol. 29, no. 3, pp. 1335–1344, May 2014.

[18] C. Su, W. Hu, Z. Chen, and Y. Hu, "Mitigation of power system oscillation caused by wind power fluctuation," *IET Renew. Power Gener.*, vol. 7, no. 6, pp. 639–651, Nov. 2013.

[19] D. Ke and C. Y. Chung, "Design of probabilistically-robust wide-area power system stabilizers to suppress inter-area oscillations of wind integrated power systems," *IEEE Trans. Power Syst.*, vol. 31, no. 6, pp. 4297–4309, Nov. 2016.

[20] A. E. Leon and J. A. Solsona, "Power oscillation damping improvement by adding multiple wind farms to wide-area coordinating controls," *IEEE Trans. Power Syst.*, vol. 29, no. 3, pp. 1356–1364, May 2014.

[21] T. Surinkaew and I. Ngamroo, "Hierarchical co-ordinated wide area and local controls of DFIG wind turbine and PSS for robust power oscillation damping," *IEEE Trans. Sustain. Energy*, vol. 7, no. 3, pp. 943–955, Jul. 2016.

[22] M. Merai, W. Naouar, I. Slama-Belkhodja, and E. Monmasson, "An adaptive PI controller design for DC-link voltage control of single-phase grid-connected converters," *IEEE Trans. Ind. Electron.*, to be published.

[23] H. S. Ramadan, A. Fathy, and M. Becherif, "Optimal gain scheduling of VSC-HVDC system sliding mode control via artificial bee colony and mine blast algorithms," *IET Gener., Transmiss. Distrib.*, vol. 12, no. 3, pp. 661–669, Feb. 2018.

[24] J. Guo, "New way to regulate DC link voltage for adaptive travel adaptor applications," in *Proc. IEEE Appl. Power Electron. Conf. Expo. (APEC)*, Charlotte, NC, USA, Mar. 2015, pp. 1924–1929.

[25] L. B. F. Leite, H. Siguerdidjane, H. D. Mathur, and Y. K. Bhateshvar, "Wind power inertial support for inter-area oscillations suppression with fuzzy controller in varying load conditions," in *Proc. Int. Conf. Clean Elect. Power (ICCEP)*, Alghero, Italy, 2013, pp. 751–754.

[26] L. Qin, J. Wang, H. Li, Y. Sun, and S. Li, "An approach to improve the performance of simulated annealing algorithm utilizing the variable universe adaptive fuzzy logic system," *IEEE Access*, vol. 5, pp. 18155–18165, 2017.

[27] B. Hoseinzadeh and Z. Chen, "Intelligent load-frequency control contribution of wind turbine in power system stability," in *Proc. Eurocon*, Zagreb, Croatia, 2013, pp. 1124–1128.

[28] J. Sun, "Impedance-based stability criterion for grid-connected inverters," *IEEE Trans. Power Electron.*, vol. 26, no. 11, pp. 3075–3078, Nov. 2011.

[29] J. Xu, B. Zhang, Q. Qian, X. Meng, and S. Xie, "Robust control and design based on impedance-based stability criterion for improving stability and harmonics rejection of inverters in weak grid," in *Proc. IEEE Appl. Power Electron. Conf. Expo. (APEC)*, Tampa, FL, USA, Mar. 2017, pp. 3619–3624.

[30] L. Qin, J. Hu, H. Li, and W. Chen, "Fuzzy logic controllers for specialty vehicles using a combination of phase plane analysis and variable universe approach," *IEEE Access*, vol. 5, pp. 1579–1588, 2017.

HAIXIN WANG received the B.Eng. degree in electrical engineering from Inner Mongolia Agricultural University, Hohhot, China, in 2011, and the M.Sc. and Ph.D. degrees in electrical engineering from the Shenyang University of Technology, Shenyang, China, in 2014 and 2017, respectively, where he is currently at the Postdoctoral Research Station. His current research interests include wind power generation systems, and power system operation and control.

JUNYOU YANG received the B.Eng. degree from the Jilin University of Technology, Jilin, China, the M.Sc. degree from the Shenyang University of Technology, Shenyang, China, and the Ph.D. degree from the Harbin Institute of Technology, Harbin, China. He was a Visiting Scholar with the Department of Electrical Engineering and Computer Science, University of Toronto, Canada, from 1999 to 2000. He is currently the Head of the School of Electrical Engineering, Shenyang University of Technology. He is also a Distinguished Professor of Liaoning province and the first hundred level candidates in the BaiQianWan Talents Program. He has led more than 50 research projects and has more than 200 publications in his technical field. His research interests include wind energy, special motor, and its control.

ZHE CHEN (M'95–SM'98) received the B.Eng. and M.Sc. degrees from the Northeast China Institute of Electric Power Engineering, Jilin, China, and the Ph.D. degree from the University of Durham, Durham, U.K. He is currently a Full Professor with the Department of Energy Technology, Aalborg University, Aalborg, Denmark. He is also the Leader of the Wind Power System Research Program at the Department of Energy Technology, Aalborg University, and the Danish Principle Investigator for Wind Energy of the Sino-Danish Centre for Education and Research. He has led many research projects and has more than 500 publications in his technical field. His research interests include power systems, power electronics, electric machines, and wind energy and modern power systems. He was an Editor of the IEEE TRANSACTIONS ON POWER SYSTEMS, an Associate Editor of the IEEE TRANSACTIONS ON POWER ELECTRONICS, a Fellow of the Institution of Engineering and Technology, London, U.K., and a Chartered Engineer in U.K.

WEICHUN GE received the B.S. and M.S. degrees from Northeast Electric Power University, China, in 1984 and 1987, respectively, and the Ph.D. degree from North China Electric Power University, Beijing, China, in 1992. He is currently a Professor of electrical engineering with Liaoning Province Electric Power Company, Shenyang, China. His research interest includes power system stability analysis.

YUNLU LI received the B.S. degree in electronic information engineering from the Shenyang University of Technology, Shenyang, China, in 2009, and the M.S. degree in control engineering and the Ph.D. degree in power electronics and drives from Northeastern University, Shenyang, in 2011 and 2017, respectively. He holds a Postdoctoral position at the School of Electrical Engineering, Shenyang University of Technology. His research interests include phase-locked loop and nonlinear filtering techniques for distributed systems and power quality.

YIMING MA received the B.Eng. degree in automation from Southwest University, Chongqing, China, in 2010, and the M.Sc. degree in electrical energy systems from Cardiff University, U.K, in 2014. He is currently pursuing the Ph.D. degree in electrical engineering with the Shenyang University of Technology, Shenyang, China. His research interest includes power quality in active distribution grid with renewable energy.

JIAN DONG received the B.S. and M.S. degrees in electrical engineering from the Shenyang University of Technology, Shenyang, China, in 2013 and 2016, respectively, where he is currently pursuing the Ph.D. degree in electrical engineering. His research interest includes power system stability analysis.

MARTIN ONYEKA OKOYE received the B.Eng. degree in electrical/electronic engineering from Nnamdi Azikiwe University, Nigeria, in 2008, and the M.Sc. degree in electronic systems design engineering from Universiti Sains Malaysia, Malaysia, in 2018. He is currently pursuing the Ph.D. degree with the Shenyang University of Technology, China. His research interests include generation systems and cyber-physical systems.

LIJIAN YANG received the B.E. degree from the Shenyang University of Technology, Shenyang, China, in 1981, and the M.S. degree from the Harbin Institute of Technology, Harbin, China, in 1984. He is currently a Professor with the Shenyang University of Technology. His research interests include nondestructive inspection, digital signal processing, and on-line testing and controlling.